J Ind Microbiol Biotechnol (2012) 39:1227–1243
DOI 10.1007/s10295-012-1115-z

METABOLIC ENGINEERING AND SYNTHETIC BIOLOGY

Metabolic flexibility of D-ribose producer strain of *Bacillus pumilus* under environmental perturbations

Rajesh K. Srivastava · Soumen K. Maiti · Debasish Das · Prashant M. Bapat · Kritika Batta · Mani Bhushan · Pramod P. Wangikar

Received: 5 September 2011 / Accepted: 27 February 2012 / Published online: 22 March 2012

Abstract The metabolic reaction rate vector is a bridge that links gene and protein expression alterations to the phenotypic endpoint. We present a simple approach for the estimation of flux distribution at key branch points in the metabolic network by using substrate uptake, metabolite secretion rate, and biomass growth rate for transketolase (*tkt*) deficient *Bacillus pumilus* ATCC 21951. We find that the glucose-6-phosphate (G6P) and pseudo catabolic/anabolic branch points are flexible in the D-ribose-producing *tkt* deficient strain of *B. pumilus*. The normalized flux through the pentose phosphate pathway (PPP) varied from 1.5 to 86 % under different growth conditions, thereby enabling substantial extracellular accumulation of D-ribose under certain conditions. Interestingly, the flux through PPP was affected by the extracellular phosphate concentration and dissolved oxygen concentration. This metabolic flexibility may have been the underlying reason for this strain being selected from thousands of others in a screening for D-ribose producers conducted in the 1970s.

Keywords Flux analysis · Transketolase deficient · D-Ribose · Sensitivity · Reliability

Abbreviation

AcCoA	Acetyl coenzyme A
Arg	Arginine
Asn	Asparagine
ADP	Adenosine 5′-diphosphate
AMP	Adenosine 5′-monophosphate
ATP	Adenosine 5′-triphosphate
CO_2	Carbon dioxide
Cys	L-Cysteine
$FADH_2$	Flavine adenine dinucleotide
G6P	Glucose-6-phosphate
Gln	L-Glutamine
Glu	L-Glutamate
Ile	L-Isoleucine
Leu	L-Leucine
Lys	L-Lysine
Met	L-Methionine
NADH	Nicotinamide adenine dinucleotide (reduced)
NADPH	Nicotinamide adenine dinucleotide phosphate (reduced)
NH_3	Ammonia
O_2	Oxygen
OA	Oxaloacetate
PDH	Pyruvate dehydrogenase
PEP	Phosphoenolpyruvate
Phe	L-Phenylalanine
PYR	Pyruvate
Pro	L-Proline
Thr	L-Threonine

Rajesh K. Srivastava and Soumen K. Maiti contributed equally.

Electronic supplementary material The online version of this article (doi:10.1007/s10295-012-1115-z) contains supplementary material, which is available to authorized users.

R. K. Srivastava
Department of Biosciences and Bioengineering, Indian Institute of Technology Bombay, Powai 400076, Mumbai, India

S. K. Maiti · D. Das · P. M. Bapat · K. Batta · M. Bhushan · P. P. Wangikar (✉)
Department of Chemical Engineering, Indian Institute of Technology Bombay, Powai 400076, Mumbai, India
e-mail: wangikar@iitb.ac.in

P. M. Bapat
Center for Mikrobiel Bioteknologi, BioCentrum-DTU, Danmarks Tekniske Universitet, Bygning 223, 2800 Kgs. Lyngby, Denmark

Tyr	L-Tyrosine
Trp	Tryptophan
UMP	Uridine-5′-monophosphate
UTP	Uridine-5′-triphosphate
Val	L-Valine
X5P	Xylulose-5-phosphate

Introduction

Metabolism is a key determinant of cellular physiology and metabolic modeling is now emerging as a tool of choice in the rational design of microbial cell factories [28, 48]. Metabolic modeling involves three key steps: (1) genome-specific metabolic reconstruction, (2) estimation of the intracellular reaction rate (flux) vector, and (3) rational modification of the genotype to affect a desired change in the flux vector [49, 52]. While methods are now available for genome-scale metabolic reconstruction [5], the subsequent tasks in metabolic modeling are not always straightforward. While direct methods of estimation of the flux vector are not currently practically feasible, the indirect methods assume that the cellular metabolites are at steady state, thereby providing a large number of constraints on the flux vector [24, 41]. Despite these constraints, the problem remains largely undetermined, necessitating additional experimental measurements or assumptions such as: (1) feeding with ^{13}C-labeled substrates and measurement of isotopic enrichment at steady state in the terminal metabolic products such as proteinogenic amino acids [7, 60], (2) linear programming-based optimization of an objective function such as the growth rate [58]. The reliability of the flux vector obtained by these methods is limited by the number of independent measurements and validity of the objective function used in optimization, respectively [42]. Further, some of the commercially interesting metabolites are produced during the slower growth phase [2, 26], which is not amenable to linear programming-based flux analysis.

Genotypic and environmental alterations invariably result in an altered flux vector [40]. The metabolic reactions can be loosely categorized into central carbon metabolism and peripheral or biosynthetic reactions. The reactions in central carbon metabolism are arranged such that there are alternatives to many reactions, a feature usually absent in the peripheral reactions [19]. Prediction of the phenotype of the mutations in the peripheral reactions is usually trivial as many of such mutations have shown a lethal phenotype [19]. However, the bow-tie architecture of the central carbon metabolism [9] coupled with the reversibility of several of the reactions makes the task of estimation of the flux vector and in turn the prediction of phenotype more challenging. Another question that is being hotly debated is about the flexibility in carbon flux partitioning at branch points in metabolic networks [19, 52]. The flux partitioning is a result of complex interplay between enzyme regulation and the rate-limiting reactions in a subnetwork [28]. Metabolic control analysis attempts to address these questions by obtaining the control coefficient for each of the reactions considered [51]. Vallino and Stephanopoulos [57] have proposed different ways to investigate the flexibility of principal branch points based on (1) attenuation of enzyme activity by the addition of a specific inhibitor, (2) amplification or attenuation of enzyme activity by genetic modification, (3) deregulation of a certain metabolite to increase metabolic burden, and (4) change in environment such as change in carbon sources.

Here we present the metabolic flux analysis of the D-ribose-producing transketolase (*tkt*) deficient strain of *Bacillus pumilus* ATCC 21951. D-Ribose is a naturally occurring sugar, found in all living organisms. D-Ribose is used as an intermediate in the production of flavor enhancers and pharmaceutically relevant products such as riboflavin (vitamin B2). Further, D-ribose is used in the treatment of myocardial ischemia and for improving the overall cardiac performance [62]. D-Ribose can be obtained by chemical or enzymatic hydrolysis of RNA [25] or by chemical synthesis from D-arabinose, D-glucose [44], or D-gluconic acid. Likewise, several naturally occurring as well as mutant strains have been reported that produce varying amounts of D-ribose [11, 53]. However, production of D-ribose by using a transketolase deficient *Bacillus* strains has proven to be the only commercially viable process [12, 23, 36]. *Tkt* is an enzyme in the non-oxidative part of the pentose phosphate pathway (PPP). The oxidative part of the PPP converts hexoses to pentoses with the loss of one molecule of carbon dioxide while the non-oxidative part effectively converts six pentose molecules to five hexose molecules. There are several other molecules and intermediates that are involved in the non-oxidative part of the PPP, which may be important as precursors for the synthesis of some of the cellular building blocks including the aromatic amino acids [6]. The non-oxidative part of the PPP is inoperative in the transketolase deficient mutants, whose direct effects include aromatic amino acid auxotrophy [29]. In addition, the mutants show several physiological characteristics, which are pleiotropically linked to the transketolase deficiency [46]. The *tkt* mutant of *B. pumilus* is known to accumulate substantial amounts of D-ribose under certain conditions [47]. Although a number of reports are available on the strain and process optimization of *tkt* deficient strains, quantification of their metabolic flux vector has not been reported.

In the present work the flexibility of principal branch points in the metabolic network of the *tkt* deficient strain of *B. pumilus* ATCC 21951 was examined. The flux vector was estimated under different media combinations including defined and semi-defined media. The effects of nutrients such as nitrogen, phosphate, and dissolved oxygen (DO) on flux partitioning at some key intracellular branch points were also examined.

Materials and methods

Organism, bioreactor, and cultivation conditions

A transketolase deficient mutant strain of *B. pumilus* ATCC 21951 was procured from the Institute for Fermentation, Osaka, Japan, catalogue number IFO 13322. The cultivation conditions were described in detail earlier [47]. The culture was maintained on agar slants containing 2.5 % Luria–Bertani broth and 2 % agar and stored at 4 °C. Three different media were used at three different stages of growth. Medium 1 consisted of 2.5 % w/v Luria–Bertani broth. Medium 2 contained the following in 1 l of distilled water: D-sorbitol, 20.0 g; corn steep liquor, 20.0 g; dipotassium hydrogen phosphate, 3.0 g; potassium dihydrogen phosphate, 1.0 g. Medium 3 contained the following in 1 l of distilled water: D-glucose with variable concentrations (40, 100, or 200 g); ammonium sulfate (AMS), 5.0 g; manganese sulfate ($MnSO_4$), 0.5 g; potassium dihydrogen phosphate, 0–1 g; calcium carbonate, 16.0 g. A loopful of the culture was transferred from an agar slant to medium 1 and grown for 24 h. This culture was then transferred to medium 2 by using 5 % v/v inoculum and grown for ca. 69 h till the culture reached post-exponential phase. This culture was then transferred to a bioreactor/shake flasks containing medium 3. Media 3 is the actual production media. Transketolase (*tkt*) deficient mutant cannot produce aromatic amino acids and therefore *tkt* deficient *Bacillus* cannot grow without aromatic amino acids in defined media. In the current work, defined production media was supplemented with small amounts of L-leucine (0.5 g l^{-1}) and aromatic amino acids L-tryptophan (0.05 g l^{-1}). For complex substrate experiments the production media were supplemented with 15 g l^{-1} casamino acid. Forty-two experiments were performed in batch cultivation either in Erlenmeyer flasks without any control of pH and dissolved oxygen or in a fermentor fitted with sensors for temperature, pH, and dissolved oxygen and a controller (Biostat® B, B. Braun Biotech International, Schwarzenberger, Germany) for controlling those parameters. The temperature of the fermentor was maintained at 37 °C. Aeration was at the rate of 1 volume of air/volume of liquid/minute (vvm). The dissolved oxygen level was maintained at 5 or 40 % by cascade control with the agitator, unless mentioned otherwise.

Analytical assays

Growth was monitored by measuring the optical density at 600 nm by using a UV–visible spectrophotometer (Model V 540, Jasco, Japan). Glucose, D-ribose, and various by-products such as acetate, acetoin, and 2,3-butanediol were estimated by HPLC (Hitachi, Merck KgaA, Darmstadt, Germany) using HP-Aminex-87-H column (Biorad Inc, USA). The temperature of the column was maintained at 65 °C. A mobile phase of 5 mM sulfuric acid was used at a flow rate of 0.6 ml min^{-1} [1]. A refractive index detector was used to detect substrate and all metabolites. Ammonium sulfate was measured using ion analyzer (EA940 Ion analyzer, Thermo Orion, USA). The concentration of free amino acids was estimated via the ninhydrin method [27]. The concentrations of individual amino acids were estimated by using the EZ-faast™ amino acid derivatization kit (Phenomenex Inc, USA) followed by detection via gas chromatography (Mak instruments, Mumbai, India) as described before [1].

Flux balance analysis

Network construction

The flux distribution through the primary metabolic pathways of the *tkt* deficient strain of *B. pumilus* ATCC 21951 was estimated from the metabolic mass balance equations based on a detailed description of the relevant metabolic reactions involved in growth and product formation. During the metabolic reconstruction process, the stoichiometry of cofactors such as NADPH, NADH, and ATP has been accounted for. All the reactions and corresponding enzymes are given as supplementary information because of space constraints. The general pathway for *B. pumilus* (KEGG: http://www.genome.jp/kegg/) was used as a starting point for the metabolic reconstruction. The glycolysis pathway (reactions R_1–R_{10}) constitutes the central route for carbon metabolism. The PPP (reactions R_{11}–R_{16}) is another important carbon dissimilation pathway. However, unlike in the wild-type strain, the PPP is not connected to the glycolysis pathway in this mutant strain due to *tkt* deficiency. Thus, linear PPP is a key characteristic of this strain. The tricarboxylic acid (TCA) cycle is another pathway for carbon breakdown, where reactions catalyzed by the enzymes citrate synthase, aconitase, NADH-dependent isocitrate dehydrogenase, oxoglutarate dehydrogenase, succinate kinase, fumarase, and malate dehydrogenase have been considered (R_{17}–R_{24}). Some of the TCA cycle intermediates are withdrawn for anabolic

purposes. For this model an important anaplerotic route for growth is pyruvate carboxylase which converts pyruvate (PYR) to oxaloacetate (OA) (R_{25}). The gluconeogenesis pathway involving phosphoenolpyruvate carboxykinase (PEP carboxykinase) has been considered where OA converts to phosphoenol pyruvate (PEP) (R_{26}). Malic enzyme (R_{27}, R_{28}) which converts PYR to malate is another important pathway. Both NADPH-dependent and NADH-dependent malate dehydrogenase are active in *B. pumilus* (KEGG: http://www.genome.jp/kegg/). Some of the extracellular metabolites such as acetate (produced via acetate kinase and phosphoacetyltransferase, R_{31} and R_{32}), acetoin and butanediol (reactions R_{29}–R_{34}) are considered. In oxidative phosphorylation, ATP is produced at the expense of NADH, $FADH_2$, and oxygen. In this study, the P/O ratio has been assumed to be constant at 1.33 [37]. The reversible transformation of reduction equivalents from NADPH to NADH takes place via transhydrogenation reactions (R_{37} and R_{38}) as also found in other gram-positive bacteria. Electron transfer from NADPH to NADH was assumed to be catalyzed in an energy-independent fashion by a soluble transhydrogenase. The reverse reaction was included as an energy-dependent reaction with a H^+-to-NADH ratio of 0.5 [22]. The Entner–Doudoroff pathway and glycoxylate shunt were not considered for network construction [55]. The amino acid biosynthesis is assumed to be similar to the pathways reported for *B. subtilis*. Reactions R_{39}–R_{41} comprise the biosynthesis of the serine family of amino acids via 3-phosphoglycerate (R_{39}), which is a commonly found intermediate for serine biosynthesis in gram-positive bacteria [45]. For cysteine (Cys) synthesis, ATP sulfurylase and adenosine-5′-phosphosulfate kinase, and enzyme activities that convert activated sulfate to sulfite and sulfide and catalyze incorporation into Cys are present in *B. subtilis* [30]. Transamination of PYR leads to biosynthesis of alanine (Ala) (R_{45}) [45]. Further, the regulation of biosynthesis of valine (Val) and leucine (Leu) in *B. subtilis* (R_{43} and R_{44}) is also reported in the literature [3]. Biosynthesis of the aspartate family of amino acids such as asparagine (Asn), lysine (Lys), threonine (Thr), methionine (Met), and isoleucine (Ile) is given in reactions R_{48}–R_{57} [31]. Transketolase deficient *B. pumilus* is not able to produce aromatic amino acids (Phe, Tyr, and Trp) because of the absence of the precursor chorismate. Glutamate (Glu) (R_{58}) and glutamine (Gln) (R_{59}) meet the requirements of amino and amide groups in cellular components. Proline (Pro) (R_{78}) and arginine (Arg) (R_{60}, R_{63}) are synthesized from glutamate [4]. Biosynthesis of nucleotides (R_{64}–R_{81}), fatty acid (R_{88}–R_{92}), and one-carbon units (R_{82}–R_{87}) were included in the model. The biomass formation equation (R_{131}) was formulated on the basis of the macromolecular composition of a related species *B. subtilis* 1012 [38, 43]. The same biomass composition was used for both the phases. The polymerization cost of ATP was calculated by Sauer et al. to be 22.387 mol ATP g-DCW^{-1} [38]. The detail of biomass formation reactions is given in the supplementary information. ATP consumption for the maintenance was expressed in the model by the conversion to ADP (R_{99}). Transport reactions of CO_2, O_2, and NH_3 from the cell to the broth and from the broth to the cell were also considered; nevertheless, their transport was assumed to be via passive diffusion.

Metabolic flux model

Quantification of the metabolic network can be achieved via flux balance analysis (FBA). The general principle of FBA has been covered extensively [50]. The reactions of the reconstructed metabolic model were formulated as a stoichiometric model $\mathbf{S} \cdot \mathbf{v} = \mathbf{0}$. This model describes cellular behavior under pseudo-steady-state conditions. **S** is the stoichiometric matrix that contains the stoichiometric coefficients of metabolite *i* in the *j*th reactions, whereas **v** is the flux vector that corresponds to the flux of the *j*th reaction. The dimension of stoichiometric matrix was 99 × 132 (i.e.,132 fluxes and 99 metabolites). The stoichiometric model was solved using linear programming, an approach often referred to as FBA [16]. The linear programming problem was formulated by defining an objective function *f*:

$$\begin{aligned} \text{Maximize } f &= \mathrm{c}\,.\,\mathrm{v} \\ \text{subject to} & \\ \mathrm{S}\,.\,\mathrm{v} &= 0 \\ lb \le v &\le ub \end{aligned} \tag{1}$$

in which *c* is a row vector containing weights of the individual variables specifying the influence of the individual fluxes on the objective function *f*. The elements of the flux vector **v** were constrained within lower limit (*lb*) and upper limit (*ub*). Uptake was defined for glucose, ammonia, amino acid, and oxygen. Secretion was defined for all major metabolic products, such as ribose, acetate, acetoin, lactate, and 2,3-butanediol. For defined media all amino acid uptake was fixed at zero. The upper bound for O_2 consumption was fixed at 20 mmol g-DCW^{-1} h^{-1} and lower limit at zero [14]. The upper bound flux for ATP maintenance was kept at 7.6 mmol g-DCW^{-1} h^{-1} and lower limit at zero [33]. All other reaction fluxes were assumed to be unbounded.

In the present study, FBA was carried out for both the phases. The objective function of growth maximization was used for the exponential growth phase (in the current study this phase will be referred to as the growth phase). However, this objective function may not be valid for the slower growth phase where product formation dominates

over growth (here termed the production phase). Therefore, an alternate objective function of minimization of error between the model predicted and experimentally measured excretion or uptake rate was used.

The nonlinear programming problem was formulated by defining an objective function h:

$$\begin{aligned} \text{Minimize } h &= \sum_{i=1}^{m} (w_{\text{i,exp}} - w_{\text{i,model}})^2 \\ &\text{subject to} \\ &\text{S.v} = 0 \\ &lb \leq v \leq ub \end{aligned} \quad (2)$$

where m is the number of measured fluxes and w is fluxes that are measured.

Simulation results obtained from these two objective functions were compared for growth phase in two of the experiments. Subsequently, the objective function of minimization of model error was used in all calculations. The linear programming tool, *linprog*, and optimization tool, *fmincon*, of the MATLAB optimization toolbox were used (MATHWORK, Natick, MA).

Sensitivity analysis and reliability of estimated flux

In order to check the reliability of the developed model, sensitivities of model responses with respect to changes in model parameter values were computed. To this end, the model parameters, i.e., internal fluxes, were changed one at a time by ±25 and ±50 % of their best fitted values obtained by solving the optimization problem given in Eq. 2. All the other internal as well as external fluxes were obtained by solving optimization problem given in Eq. 2 while keeping the single internal flux fixed. The sensitivities of the external fluxes to changes in the internal fluxes were thus obtained by computing the following ratio: $\frac{w(v_i+\delta v_i)-w(v_i)}{w(v_i)} \times 100\,\%$ where $w(v_i)$ represents the simulated values of external flux w with estimated ith internal flux value v_i and $w(v_i + \delta v_i)$ simulated values of external flux w when ith internal flux value v_i is perturbed.

It is expected that for a sensible model, the external fluxes will be sensitive to some of the internal fluxes.

Similar to the above analysis for model validation, extensive statistical analyses were performed to investigate the reliability of estimated fluxes determined for different environmental perturbations. This is necessary to ensure that the experimental errors which are intrinsic to experimental measurements do not unduly affect the estimated fluxes. For this reliability analysis, 400 simulated measurement data sets of specific biomass growth rate and specific extracellular metabolite production rate were generated by addition of randomly generated, zero-mean, normally distributed measurement noise (with variance 0.01 for specific growth rate, 0.1 for specific metabolite secretion and specific substrate uptake rate) to the experimentally measured data set corresponding to different environmental conditions and different growth phases. It should be noted that the variance of the perturbations thus induced in the measurement data is much higher than the noise variances as determined from repeated experimental measurements. The "model error minimization" based optimization routine (Eq. 2) was applied to estimate the flux distribution from each of the 400 simulated measurement data sets for different environmental conditions and growth phases.

Confidence intervals based on the percentile method [13] were calculated were calculated as the distribution of the data set and population variance is unknown. The $(1 - \alpha)$ percent confidence interval of a parameter is then estimated by considering the $\alpha/2$ and $(1 - \alpha/2)$ percentiles of the data set as the lower and upper limits of the confidence interval, respectively. The internal fluxes with low width confidence intervals can be said to have been estimated with high reliability.

Results

It was of interest to examine the flexibility of the metabolic network of the D-ribose producer strain of *B. pumilus* under environmental perturbations. To that end, biomass growth, substrate consumption, and product formation profiles were analyzed under 42 different media compositions. Of these, nine media compositions were completely defined or semi-defined and hence were amenable to flux analysis. Amongst these, seven media compositions showed two distinct growth phases, namely growth phase where growth rate is high and production phase where growth rate is slower but ribose production rate is higher, whereas two of the media compositions showed only a single growth phase that we have defined as growth phase. Flux analysis was carried out in both the phases for these former seven batches, thereby resulting in pseudo-steady-state flux values under 16 (7 batches × 2 phases and 2 batches × 1 phase) different culture conditions.

Initially the flux values and specific growth rates were estimated via the two objective functions, maximization of growth and minimization of model error, for the two media compositions that showed relatively high specific growth rates. Note that the predicted specific growth rate values are comparable to the experimental values in both the experiments in growth phases (Table 1), thereby validating the metabolic model used in this study. But the predicted growth rates in the production phase using the objective function maximization of growth were significantly

Table 1 Comparison of metabolic flux values obtained via two different objective functions, maximization of growth and minimization of model error

Medium composition	Maximization of growth					Minimization of model error					Experimentally measured
	Flux value (mmol g-biomass^{-1} h^{-1})					Flux value (mmol g-biomass^{-1} h^{-1})					
	Glucose	PPP	TCA	PDH	μ (h^{-1})	Glucose	PPP	TCA	PDH	μ (h^{-1})	μ (h^{-1})
Casamino acids (15 g l^{-1}), glucose (200 g l^{-1}), and ammonium sulfate (5 g l^{-1})[a]	2.11	0.71	0.45	1.28	0.27	2.11	0.7	0.44	1.33	0.25	0.25 ± 0.03
Glucose (200 g l^{-1}) and ammonium sulfate (5 g l^{-1})[a]	3.35	0.89	0.66	1.03	0.22	3.35	0.88	0.66	1.13	0.21	0.21 ± 0.02

PPP pentose phosphate pathway, *TCA* tricarboxylic acid cycle, *PDH* pyruvate dehydrogenase, μ specific growth rate

[a] Additional medium components (in 1 l of distilled water): manganese sulfate, 0.5 g; calcium carbonate, 16.0 g; L-leucine, 0.5 g; L-tryptophan, 0.05 g

different from experimental values (data not shown). Hence, as the objective function of maximization of growth may not be valid in the production phase, we compared the metabolic flux values obtained by using this objective function with those obtained by using the objective function of minimization of model error. The flux values obtained by the two objective functions were found to be comparable for the key metabolic reactions in the growth phase (Table 1; Fig. 1). On the basis of this result, the objective function of minimization of model error was used for all subsequent analyses. Therefore this objective function can be used for both growth phase and stationary phase.

Statistical analysis

To check the reliability of the developed model, simulations were performed to determine the sensitivity of extracellular metabolites and biomass formation rate to changes in internal fluxes. Sensitivity analysis revealed that the measured extracellular fluxes were sensitive to several internal fluxes, thereby increasing confidence in the flux balance model. Perturbation effects of two such sensitive fluxes—pyruvate dehydrogenase (R_{10}) and 2-ketoglutarate dehydrogenase (R_{20})—are shown in Table 2. These results indicate that the measured extracellular fluxes were sensitive to the flux change of pyruvate dehydrogenase and 2-ketoglutarate dehydrogenase for different experiments and different phases.

Additional statistical analysis, as discussed in the "Materials and methods" section, was performed to compute the uncertainty of the computed internal fluxes. In particular, 95 % confidence limits obtained using the percentile method for the estimated fluxes were adopted to evaluate the quality of the estimates. A total of 400 simulated measurement datasets were used for each experiment and each phase. The generation of these datasets has been described earlier.

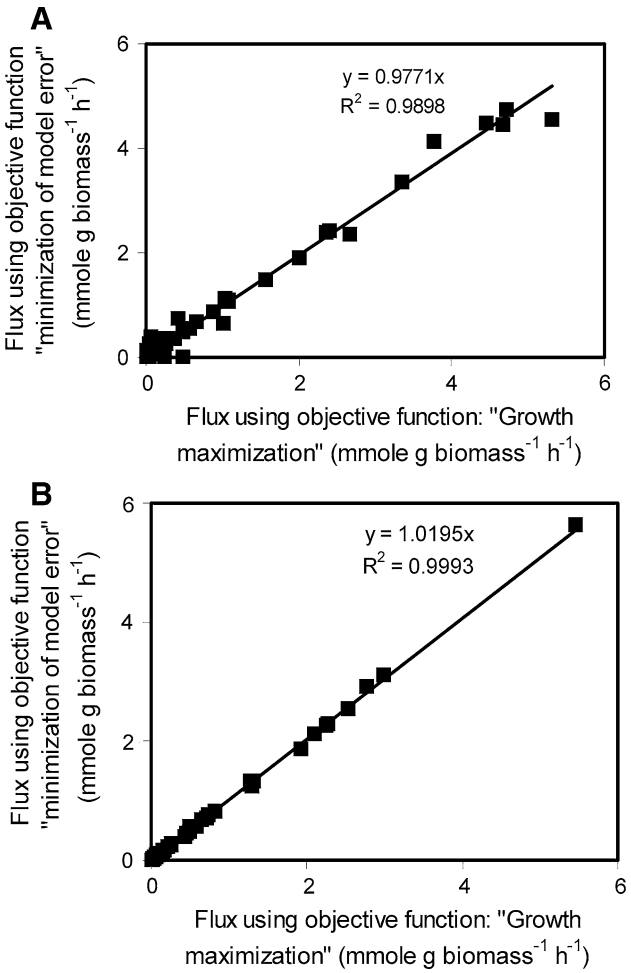

Fig. 1 Comparison of the intracellular reaction rates of the transketolase deficient strain of *B. pumilus* ATCC 21951 obtained by using two different objective functions, maximization of biomass and minimization of model error. **a** Experiments in shake flasks in medium containing 200 g l^{-1} glucose and 15 g l^{-1} casamino acid. **b** Experiments in shake flasks in medium containing 200 g l^{-1} glucose. Additional medium components (in 1 l of distilled water): ammonium sulfate, 5 g; manganese sulfate, 0.5 g; calcium carbonate, 16.0 g; L-leucine, 0.5 g; L-tryptophan, 0.05 g. *PPP* pentose phosphate pathway, *TCA* tricarboxylic acid cycle, *PDH* pyruvate dehydrogenase

Table 2 Sensitivity of model responses with respect to change in different reactions

Experiment	Perturbation (%)	μ	q_{glu}	q_{rib}	q_{ac}	q_{act}	q_{but}
Perturbation of R_{10} (pyruvate dehydrogenase: PYR to AcCoA formation)							
100 g l^{-1} Glucose in shake flasks[a]	−50	0.42 (0.11)	4.79 (4.87)	1.23 (1.92)	0.00 (0.01)	0.09 (1.30)	0.04 (0.25)
	−25	0.31 (0.04)	4.87 (4.89)	1.21 (1.90)	0.00 (0.00)	0.06 (1.27)	0.02 (0.23)
	0	0.19 (0.01)	4.89 (4.90)	1.18 (1.89)	0.00 (0.00)	0.04 (1.26)	0.00 (0.22)
	+25	0.08 (0.00)	4.92 (5.04)	1.16 (1.76)	0.00 (0.00)	0.02 (1.11)	0.00 (0.07)
	+50	0.00 (0.00)	5.11 (5.21)	1.03 (1.65)	0.00 (0.01)	0.00 (0.98)	0.00 (0.00)
200 g l^{-1} Glucose in shake flasks[a]	−50	0.14 (0.11)	3.21 (2.68)	0.81 (0.77)	0.11 (0.42)	1.21 (0.65)	0.16 (0.08)
	−25	0.17 (0.07)	3.32 (2.69)	0.79 (0.76)	0.30 (0.41)	1.13 (0.64)	0.07 (0.07)
	0	0.20 (0.02)	3.35 (2.71)	0.66 (0.75)	0.37 (0.41)	1.07 (0.63)	0.02 (0.06)
	+25	0.18 (0.00)	3.37 (2.75)	0.64 (0.70)	0.38 (0.43)	1.06 (0.58)	0.01 (0.02)
	+50	0.15 (0.01)	3.41 (4.91)	0.62 (1.98)	0.35 (0.21)	1.04 (0.03)	0.003 (1.1)
100 g l^{-1} Glucose, 0.5 KH_2PO_4	−50	0.41 (0.07)	6.21 (3.34)	1.13 (2.00)	0.00 (0.00)	0.82 (0.51)	0.07 (0.17)
in shake flasks[a]	−25	0.23 (0.05)	6.31 (3.11)	1.1 (1.98)	0.00 (0.00)	0.78 (0.48)	0.03 (0.16)
	0	0.05 (0.02)	6.41 (3.32)	1.04 (1.97)	0.001 (0.0)	0.74 (0.47)	0.01 (0.15)
	+25	0.0 (0.001)	6.72 (3.33)	0.78 (1.95)	0.00 (0.00)	0.46 (0.46)	0.00 (0.13)
	+50	0.00 (0.00)	7.13 (3.36)	0.42 (1.93)	0.00 (0.00)	0.10 (0.42)	0.00 (0.10)
Perturbation of R_{20} (2-ketoglutarate dehydrogenase: AKG to SUCCoA formation)							
100 g l^{-1} Glucose in shake flasks[a]	−50	0.36 (0.11)	4.87 (4.84)	1.21 (1.93)	0.012 (0.008)	0.07 (1.28)	0.02 (0.24)
	−25	0.28 (0.06)	4.88 (4.88)	1.20 (1.91)	0.006 (0.004)	0.06 (1.27)	0.01 (0.23)
	0	0.20 (0.01)	4.90 (4.90)	1.19 (1.90)	0.00 (0.00)	0.04 (1.26)	0.00 (0.22)
	+25	0.11 (0.00)	4.91 (5.00)	1.18 (1.82)	0.00 (0.00)	0.03 (1.18)	0.00 (0.14)
	+50	0.03 (0.00)	4.96 (5.11)	1.16 (1.74)	0.00 (0.00)	0.02 (0.99)	0.00 (0.06)
200 g l^{-1} Glucose in shake flasks[a]	−50	0.22 (0.09)	3.351 (2.75)	0.667 (0.75)	0.370 (0.43)	1.072 (0.59)	0.014 (0.03)
	−25	0.207 (0.03)	3.345 (2.69)	0.672 (0.77)	0.366 (0.44)	1.072 (0.69)	0.012 (0.09)
	0	0.202 (0.02)	3.351 (2.71)	0.666 (0.75)	0.370 (0.41)	1.071 (0.63)	0.013 (0.06)
	+25	0.198 (0.00)	3.352 (2.72)	0.666 (0.72)	0.370 (0.40)	1.071 (0.61)	0.013 (0.04)
	+50	0.195 (0.00)	3.346 (2.8)	0.666 (0.67)	0.370 (0.37)	1.070 (0.55)	0.012 (0.00)
100 g l^{-1} Glucose, 0.5 KH_2PO_4	−50	0.342 (0.06)	6.324 (3.27)	1.103 (1.99)	0.022 (0.003)	0.788 (0.49)	0.045 (0.17)
in shake flasks[a]	−25	0.195 (0.04)	6.347 (3.28)	1.081 (1.98)	0.011 (0.001	0.766 (0.48)	0.022 (0.16)
	0	0.048 (0.02)	6.369 (3.30)	1.058 (1.97)	0.00 (0.00)	0.744 (0.47)	0.00 (0.15)
	+25	0.00 (0.005)	6.623 (3.32)	0.749 (1.95)	0.00 (0.00)	0.558 (0.45)	0.00 (0.14)
	+50	0.00 (0.00)	6.973 (3.41)	0.454 (1.92)	0.00 (0.00)	0.139 (0.44)	0.00 (0.12)

All results are given in units of mmol g-DCW^{-1} h^{-1}. Data outside parentheses are for growth phase and data within parentheses are for production phase

AKG α-ketoglutarate, *SUCCoA* succinyl coenzyme A; μ, q_{glu}, q_{rib}, q_{ac}, q_{act}, and q_{but} denote the specific growth rates, specific glucose consumption rate, specific D-ribose, acetate, acetoin, and 2,3-butanediol formation rate, respectively

[a] Additional medium components (in 1 l of distilled water): ammonium sulfate, 5 g; manganese sulfate, 0.5 g; calcium carbonate, 16.0 g; L-leucine, 0.5 g; L-tryptophan, 0.05 g

On the basis of these simulations, the computed confidence intervals of fluxes for which the measured extracellular fluxes had high sensitivity are presented in Table 3. The widths of the confidence intervals of these fluxes are low, thereby indicating that these fluxes are estimated with low uncertainty.

Flexibility of metabolic network

To analyze the flexibility of the metabolic network, histograms of the relative values of intracellular fluxes (Fig. 2b, f), absolute values of excretion or uptake rates (Fig. 2g, h), specific growth rate (Fig. 2j), and relative product yields (Fig. 2i, k–m) were generated. All 42 experimental datasets were used to construct histograms of extracellular metabolites secretion, uptake rates, and specific growth rates and nine experiments (both phases) were used to construct histograms of intracellular fluxes. We observe a large variation in the absolute values of the excretion or uptake rates and specific growth rate (μ) depending on the medium composition and the growth stage. For example, μ varies

Table 3 Confidence interval of sensitive intracellular fluxes at 95 % confidence level

Reaction number[a]	Media: 200 g l^{-1} glucose + 5 g l^{-1} AMS[b]				Media: 100 g l^{-1} glucose + 5 g l^{-1} AMS + 0.5 g l^{-1} KH_2PO_4[b]				Media: 200 g l^{-1} glucose + 5 g l^{-1} AMS + 15 g l^{-1} casamino acid[b]			
	Growth phase		Production phase		Growth phase		Production phase		Growth phase		Production phase	
	[LB UB]	Optimal	[LB UB]	Optimal	[LB UB]	Optimal	[LB UB]	Optimal	[LB UB]	Optimal	[LB UB]	Optimal
R2	[71.1 73.5]	72.2	[70.3 72.9]	71.2	[82.0 82.9]	82.4	[38.6 40.5]	39.5	[62.5 64.1]	63.2	[57.6 58.6]	58.0
R3	[69.7 72.4]	71.0	[70.1 71.9]	71.0	[81.8 82.8]	82.2	[38.5 40.3]	39.4	[60.0 61.7]	60.8	[57.4 58.4]	57.8
R6	[138.9 144.3]	141.6	[140.1 143.9]	142.0	[163.6 165.6]	164.4	[76.9 80.5]	78.7	[119.0 122.3]	120.6	[114.7 116.8]	115.7
R8	[131.3 136.8]	133.9	[138.9 143.2]	141.1	[162.5 165.0]	163.5	[76.0 79.6]	77.8	[106.8 109.7]	108.2	[113.7 115.8]	114.7
R9	[130.6 136.1]	133.2	[147.0 154.0]	150.8	[186.4 192.0]	189.0	[76.1 80.5]	78.1	[105.3 108.2]	106.7	[130.3 135.2]	133.4
R10	[26.8 36.3]	33.7	[80.3 89.2]	85.2	[133.4 138.6]	135.8	[33.0 37.9]	35.3	[61.9 64.1]	63.1	[72.4 75.8]	73.9
R11	[24.9 27.1]	26.1	[27.8 29.4]	28.5	[16.9 17.7]	17.3	[59.3 61.1]	60.2	[32.4 34.1]	33.3	[41.1 42.2]	41.6
R12	[24.9 27.1]	26.1	[27.8 29.4]	28.5	[16.9 17.7]	17.3	[59.3 61.1]	60.2	[32.4 34.1]	33.3	[41.1 42.2]	41.6
R13	[24.9 27.1]	26.1	[27.8 29.4]	28.5	[16.9 17.7]	17.3	[59.3 61.1]	60.2	[32.4 34.1]	33.3	[41.1 42.2]	41.6
R15	[18.4 21.2]	19.8	[27.2 28.5]	27.8	[16.3 16.9]	16.6	[58.6 60.4]	59.4	[19.8 21.7]	20.8	[40.1 41.2]	40.7
R16	[18.4 21.2]	19.8	[27.2 28.5]	27.8	[16.3 16.9]	16.6	[58.6 60.4]	59.4	[19.8 21.7]	20.8	[40.1 41.2]	40.7
R18	[5.30 12.9]	10.3	[62.4 72.9]	68.2	[131.4 137.5]	134.3	[31.6 36.4]	33.8	[35.1 36.8]	36.0	[55.6 59.4]	57.4
R19	[5.30 12.9]	10.3	[62.4 72.9]	68.2	[131.4 137.5]	134.3	[31.6 36.4]	33.8	[35.1 36.8]	36.0	[55.6 59.4]	57.4
R20	[0.0 6.5]	3.8	[61.1 72.6]	67.4	[130.3 137.0]	133.5	[30.7 35.6]	33.0	[25.7 27.0]	26.4	[54.7 59.4]	56.5
R21	[0.0 6.5]	3.8	[61.1 72.6]	67.4	[130.3 137.0]	133.5	[30.7 35.6]	33.0	[25.7 27.0]	26.4	[54.7 58.6]	56.5
R22	[0.0 6.5]	3.8	[61.1 72.6]	67.4	[130.3 137.0]	133.5	[30.7 35.6]	33.0	[25.7 27.0]	26.4	[54.7 58.6]	56.5
R25	[15.55 21.3]	19.3	[74.1 84.0]	79.9	[158.1 165.9]	161.8	[33.4 39.2]	36.2	[26.3 27.3]	26.8	[74.1 58.6]	78.3
R26	[0.0 0.12]	0	[6.4 10.8]	9.7	[23.9 27.3]	25.5	[0.0 1.3]	0.4	[0.0 0.0]	0	[15.6 19.4]	18.8
R28	[0.0 1.99]	0	[61.8 72.2]	67.9	[130.9 137.3]	133.9	[30.6 36.1]	33.5	[0.0 0.4]	0	[54.4 58.8]	57.0
R36	[0.0 6.5]	3.8	[61.1 69.5]	67.4	[130.3 137.0]	132.5	[30.7 35.6]	33.1	[25.7 27.1]	26.4	[54.7 58.6]	56.5
R73	[15.7 24.8]	22.0	[78.1 88.5]	84.4	[122.1 129.0]	125.3	[49.2 52.7]	50.9	[19.0 19.6]	19.3	[70.3 72.7]	71.4

LB lower bound and *UB* upper bound

[a] See supplementary information for reaction number

[b] Additional medium components (in 1 l of distilled water): manganese sulfate, 0.5 g; calcium carbonate, 16.0 g; L-leucine, 0.5 g; L-tryptophan, 0.05 g in shake flasks for defined media and manganese sulfate, 0.5 g; calcium carbonate, 16.0 g for casamino acid experiment

from 0.04 to 0.32 h^{-1} (Fig. 2j) whereas the specific glucose uptake rate varies from 0.5 to 6.6 mmol g-DCW^{-1} h^{-1} (Fig. 2h). Further, we analyzed the relative flux through a given pathway at some of the key branch points in the network. The relative flux through the PPP varies from 1.5 to 86 % (Fig. 2b), whereas the relative flux through TCA cycle varies from 14 to 90 % (Fig. 2c). However, the variation in the relative fluxes through pyruvate dehydrogenase, and anaplerotic and gluconeogenesis pathways was comparatively less (Fig. 2d–f). This indicates that the metabolic network of the organism is inherently flexible at some of the branch points. The yields of some of the products are indicative of flux through a given metabolic pathway. D-Ribose yield, which is qualitative indicator of the relative flux through PPP, varied from 0 to 75 % in the 42 experiments (Fig. 2i). Likewise, the yields of the other metabolic products varied substantially (Fig. 2k–m).

In FBA, the distribution of fluxes at some key branch points is usually considered. To this end, we analyzed the flux distribution at four key branch points in the network. We found that the catabolic flux partitioning between glycolysis and PP pathway at the G6P node is flexible as the outgoing flux was not correlated with incoming flux (Fig. 3a). It has been observed that in this strain the specific growth rate is not regulated by pentose phosphate (PP) pathway (Fig. 3b). This suggests that the G6P branch point provides the cell with the flexibility to regulate the energy and intermediate fluxes under environmental perturbations. Another key branch point is acetyl coenzyme A, with the primary incoming flux through pyruvate dehydrogenase (PDH) and outgoing flux toward the TCA cycle or acetate. The fluxes through PDH and citrate synthase, the primary incoming and outgoing fluxes, were highly correlated (Fig. 3c). In contrast to the G6P branch point, flux partitioning at AcCoA was rigid with a high degree of correlation between the incoming and outgoing fluxes (Fig. 3c). Another branch point is PYR with incoming fluxes via pyruvate kinase and malic enzyme and outgoing fluxes via PDH, pyruvate carboxylase, and acetolactate synthase. The PYR branch point was found to be rigid with a high correlation between incoming and outgoing fluxes (Fig. 3d, e). There are some branch points in the central carbon pathway where the biosynthetic fluxes diverge [19]. Thus, the partitioning of glucose to the anabolic biomass or catabolic product/by-product can be considered as a pseudo-branch point (Fig. 3f). The flux into biomass was not correlated to the glucose uptake rate and is indicative of flexibility in the biosynthetic network.

Flux distribution at key branch points

It was of interest to ascertain the effect of various medium components on the flux distribution at some of the key branch points. To that end, we analyzed the effect of the concentrations of glucose, inorganic phosphate, and dissolved oxygen on the flux distribution in minimal media.

Effect of glucose on flux distribution

Glucose concentration had a substantial effect on product, growth, and by-product formation in *tkt* deficient *B. pumilus* culture (Fig. 4). The productivity was higher in 100 g l^{-1} glucose compared to both 40 and 200 g l^{-1} glucose media but the biomass concentration was higher in 200 g l^{-1} glucose media. The growth profiles were divided into two regions: the growth and production phases. Growth rate is high at 12–48 h in 40 and 100 g l^{-1} glucose media and at 36–72 h in 200 g l^{-1} glucose media with very low ribose production. This phase is termed the growth phase. Ribose production rate is very high in the period 48–72 h in 40 and 100 g l^{-1} glucose media and 72–98 h in 200 g l^{-1} glucose media. This phase is termed the production phase (Fig. 4). The specific growth rates, specific glucose consumption rate, and specific D-ribose, acetate, acetoin, and 2,3-butanediol formation rates in both phases were used for flux analysis. These data are presented in the supplementary information. Flux through PPP in the growth phase was higher in 100 g l^{-1} glucose media compare to both 40 and 200 g l^{-1} glucose media in shake flasks (Fig. 5a). A similar pattern of flux distribution was observed in the production phase. Further, the flux through the gluconeogenesis pathway was completely suppressed at a glucose concentration of 200 g l^{-1}. The ATP maintenance requirement was found to be in general greater in the production phase as compared to the corresponding growth phase. The transhydrogenase activity was found to be relatively high in the reverse direction from NADH to NADPH in all cases. Note that these experiments were conducted in Erlenmeyer flasks incubated in a shaker, where normally the dissolved oxygen concentration is much lower than in an aerated fermentor.

Effect of dissolved oxygen on flux distribution

The effect of dissolved oxygen concentration was ascertained by conducting the experiments in a sensor-equipped fermentor where the DO was maintained at 5 or 40 % of saturation and glucose concentration varied from 100 to 200 g l^{-1} in glucose media with and without supplementing with 15 g l^{-1} casamino acid. All the experiments were carried out in triplicate. Irrespective of the presence of casamino acid, when the DO was maintained at 40 % and glucose concentration at 100 g l^{-1} there was no production of ribose. However, in media containing 5 % DO with 100 g l^{-1} glucose or 40 % DO with 200 g l^{-1} glucose (data not shown), ribose was produced and the PPP was

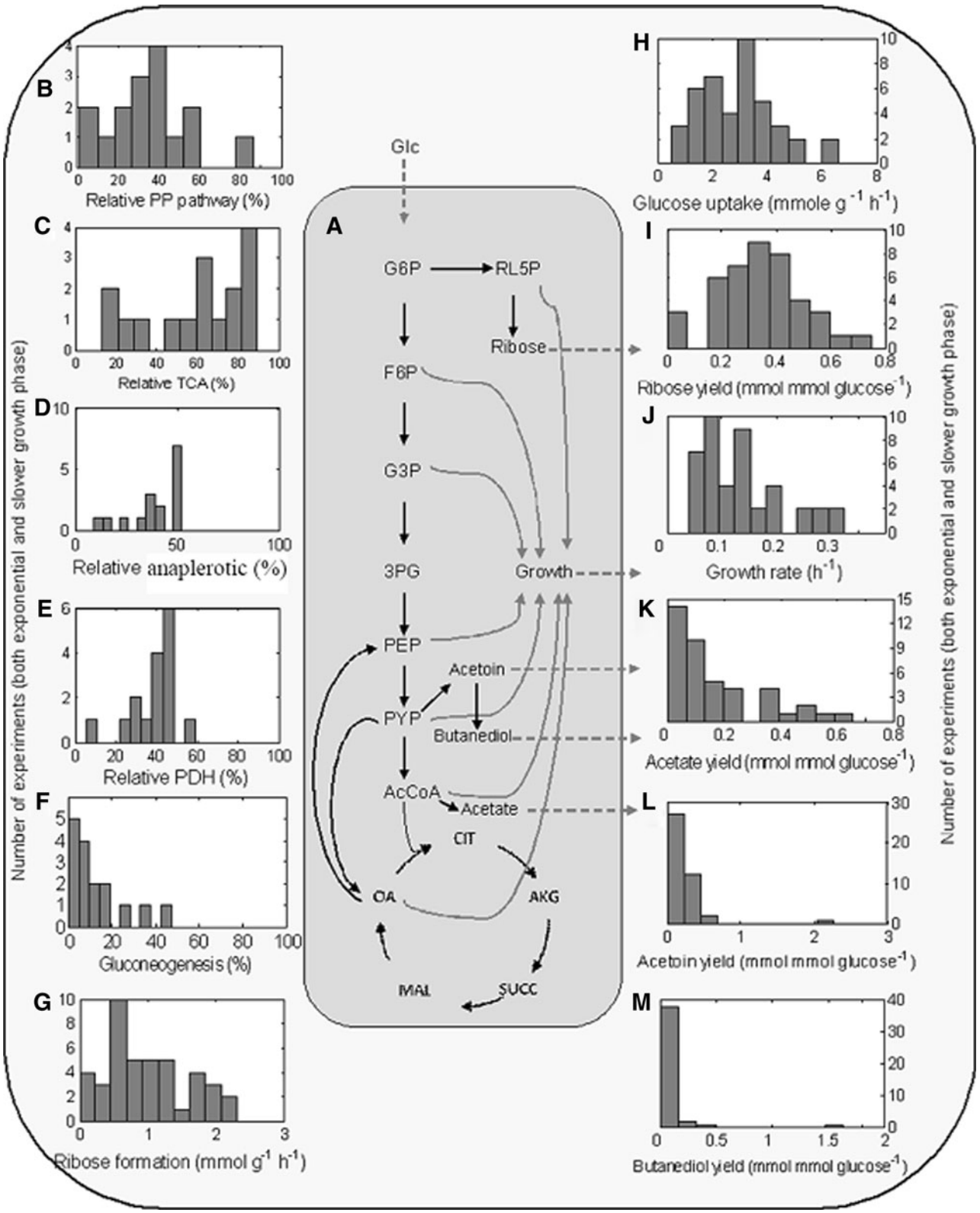

Fig. 2 Distribution of the relative and absolute values of metabolic fluxes in *B. pumilus* ATCC 21951. The relative flux value is calculated by dividing the outgoing flux by all the incoming fluxes for the respective branch point. **a** Condensed view of the metabolic network used in the study; **b** relative PP pathway; **c** relative TCA; **d** relative anaplerotic; **e** relative PDH; **f** gluconeogenesis; **g** ribose formation; **h** glucose uptake; **i** ribose yield; **j** specific growth rate; **k** acetate yield; **i** acetoin yield; and **m** butanediol yield. Relative fluxes distribution designed on the basis of nine experiments (both the growth phases) and other distribution designed on the basis of 42 experiments

active irrespective of the presence or absence of casamino acid. Note that the ribose production at 40 % DO with 200 g l^{-1} glucose was higher compared to production at 5 % DO with 100 g l^{-1} glucose. Thus, the flux through the PPP is not only dependent on DO and glucose concentration, but also depends on the glucose/oxygen ratio. Flux analysis was carried out in 40 % DO with 100 g l^{-1} without supplementing with casamino acid (Fig. 5). The PPP was almost repressed except the flux from R5P for biomass, with the majority of the flux being channeled through glycolysis. Likewise, there was a substantial increase in the flux through the TCA cycle under these conditions. These results point toward a strong correlation between the PPP flux and the ratio of glucose and DO in the medium.

Effect of phosphate on flux distribution

Phosphate is known to alter intracellular fluxes in several organisms [10]. In the mutant strain being used in this study, the effect of phosphate on intracellular fluxes can be even more pronounced due to the fact that the strain is deficient in some membrane lipids such as teichoic acid, teichuronic acid, and lipoteichoic acids [34, 35]. The intracellular flux pattern was substantially affected by the inorganic phosphate concentration in the media (Fig. 5b).

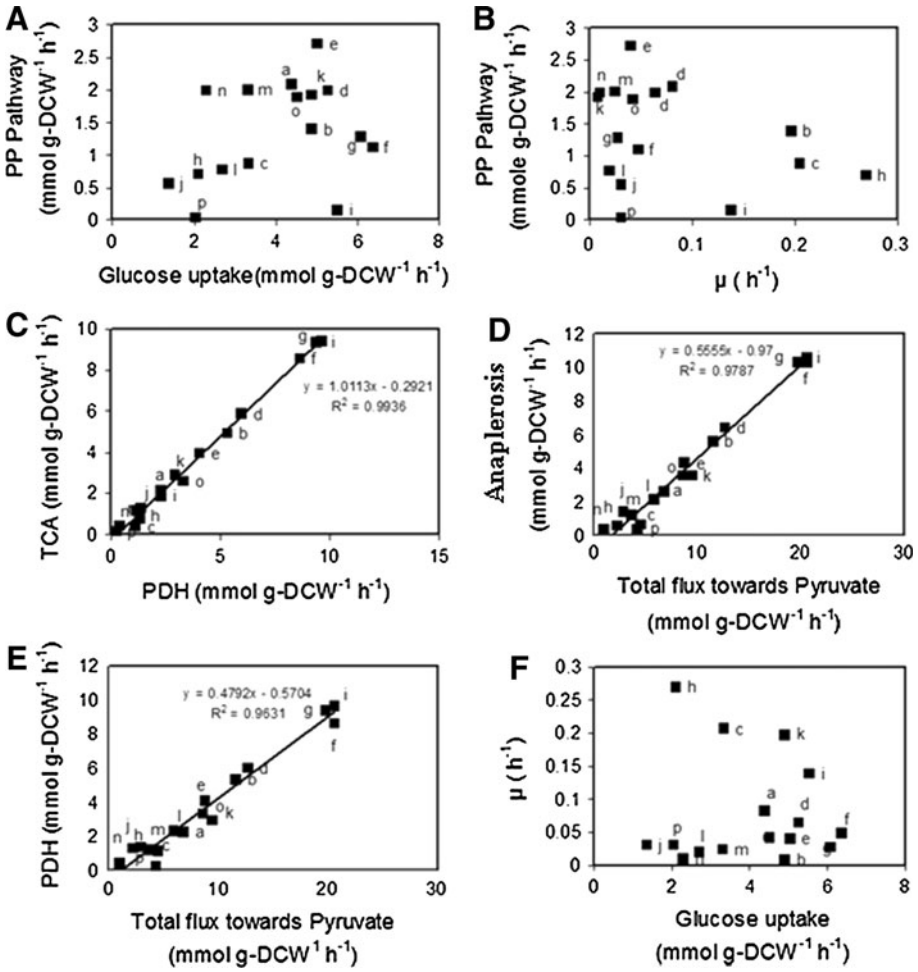

Fig. 3 Absolute flux at four key branch points. **a** and **b** Glucose 6 phosphate, **c** acetyl CoA, **d** and **e** pyruvate, and **f** growth branch point. *a* 40 g l^{-1} glucose, 5 g l^{-1} AMS in shake flasks—growth phase. *b* 100 g l^{-1} glucose, 5 g l^{-1} AMS in shake flasks—growth phase. *c* 200 g l^{-1} glucose, 5 g l^{-1} AMS in shake flasks—growth phase. *d* 100 g l^{-1} glucose, 5 g l^{-1} AMS, 0.1 g l^{-1} KH_2PO_4 in shake flasks—growth phase. *e* 100 g l^{-1} glucose, 5 g l^{-1} AMS, 0.2 g l^{-1} KH_2PO_4 in shake flasks—growth phase. *f* 100 g l^{-1} glucose, 5 g l^{-1} AMS, 0.5 g l^{-1} KH_2PO_4 in shake flasks—growth phase. *g* 100 g l^{-1} glucose, 5 g l^{-1} AMS, 1.0 g l^{-1} KH_2PO_4 in shake flasks—growth phase. *h* 200 g l^{-1} glucose, 5 g l^{-1} AMS, 15 g l^{-1} casamino acid in shake flasks—growth phase. *i* 100 g l^{-1} glucose, 5 g l^{-1} AMS in fermentor 40 % DO—growth phase. *j* 40 g l^{-1} glucose, 5 g l^{-1} AMS in shake flasks—production phase. *k* 100 g l^{-1} glucose, 5 g l^{-1} AMS in shake flasks—production phase. *l* 200 g l^{-1} glucose, 5 g l^{-1} AMS in shake flasks—production phase. *m* 100 g l^{-1} glucose, 5 g l^{-1} AMS, 0.5 g l^{-1} KH_2PO_4 in shake flasks—production phase. *n* 100 g l^{-1} glucose, 5 g l^{-1} AMS, 1.0 g l^{-1} KH_2PO_4 in shake flasks—production phase. *o* 200 g l^{-1} glucose, 5 g l^{-1} AMS, 15 g l^{-1} casamino acid in shake flasks—production phase. *p* 100 g l^{-1} glucose, 5 g l^{-1} AMS in fermentor 40 % DO—production phase. Refer to legend of Fig. 1 for additional media components

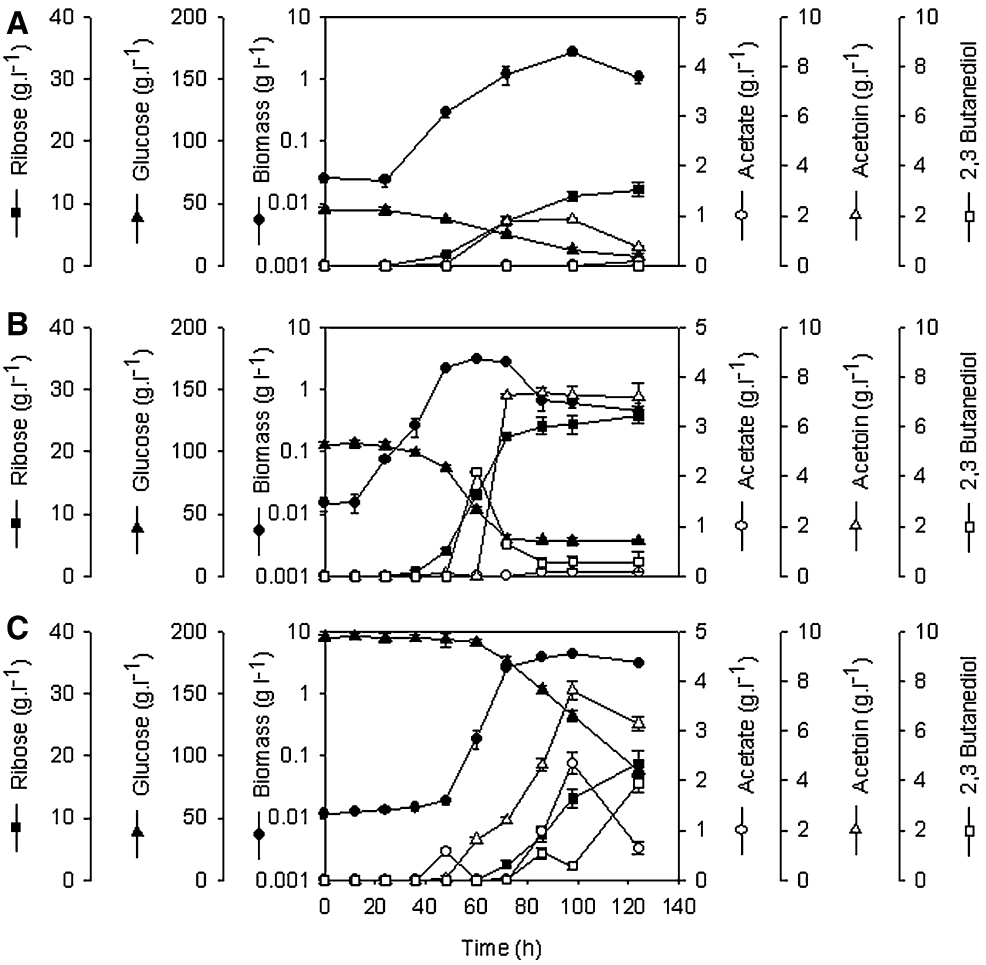

Fig. 4 Effect of glucose concentration on growth, product, and by-product formation in production media of transketolase deficient strain of *B. pumilus* ATCC 21951 using shake flasks. **a** Glucose 40 g l^{-1}, **b** glucose 100 g l^{-1}, and **c** glucose 200 g l^{-1}. The unit of butanediol is g l^{-1}. Refer to legend of Fig. 1 for additional media components

With KH_2PO_4 concentrations of 0.1 and 0.2 g l^{-1}, only a single constant growth phase was detected, which lasted for approximately 120 h. Therefore the flux distribution was calculated for a single phase for these experiments. The glucose uptake increases in the presence of phosphate in the media. The absolute glucose uptake rate increased from 2.5 to 6.5 mol g-DCW^{-1} h^{-1} with increasing phosphate concentration (see supplementary material). The flux through the PPP was higher at low KH_2PO_4 concentration compared to media with excess KH_2PO_4 in the growth phase (Fig. 4b). This is consistent with reported literature where PPP flux was higher under phosphorus-limited conditions for *B. subtilis* [10]. However, with 0.5 and 1.0 g l^{-1} phosphate concentrations, the flux through the PPP was much higher in the production phase (Fig. 5b). The TCA flux is low in phosphorus-limited culture which is consistent with phosphorus-limited culture of *B. subtilis* [10]. Likewise, we observed large variations in glycolytic flux from 45.8 to 82.4 % in media containing different phosphate concentrations. The fluxes through glyceraldehyde-3-phosphate dehydrogenase (EC 1.2.1.12) were decreased at low KH_2PO_4 concentration as the glyceraldehyde-3-phosphate dehydrogenase is inhibited at low phosphate concentrations [8, 18, 59]. The gluconeogenesis flux from OA to PEP catalyzed by PEP carboxykinase was very low at lower concentration of phosphate compared to media with excess KH_2PO_4 in the growth phase (Fig. 4a, b). This agrees with the reported results for *B. subtilis* [10]. Malic enzyme activity and anaplerosis flux were lower with 0.2 g l^{-1} KH_2PO_4 compared to other phosphate concentrations.

Flux distribution in semi-defined media

Next, we analyzed the flux distribution in semi-defined media containing casamino acids. The uptake rates of the various amino acids were measured and accounted for while establishing the carbon balance in the network. While the specific growth rate was higher, the glucose uptake rate was lower than the corresponding values for minimal medium. This may be due to the fact that the organism takes up amino acids along with glucose in the initial phase of growth. Subsequently, the glucose uptake rate increases as the amino acids get consumed. The fluxes through PPP, PDH, and malic enzyme are higher in both the phases than those in defined medium (Fig. 6). The

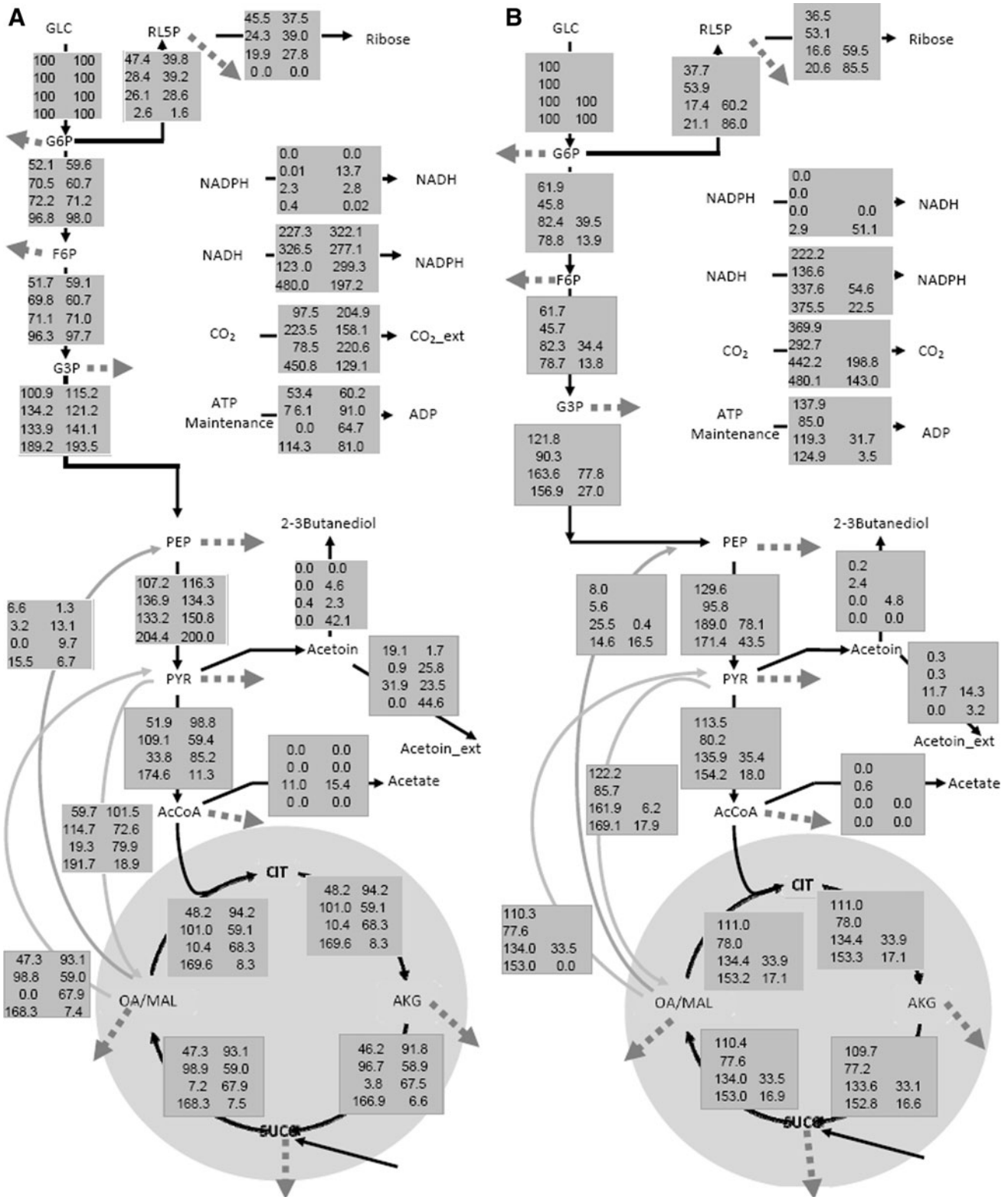

Fig. 5 Flux distribution of *B. pumilus* network. **a** Metabolic flux distribution in defined media without inorganic phosphate. *First row* 40 g l^{-1} glucose, *second row* 100 g l^{-1}, *third row* 200 g l^{-1} in shake flasks, *fourth row* 100 g l^{-1} glucose in fermentor at 40 % dissolved oxygen concentration. **b** Metabolic flux distribution in defined media with inorganic phosphate. *First row* 0.1 g l^{-1} KH_2PO_4, *second row* 0.2 g l^{-1} KH_2PO_4, *third row* 0.5 g l^{-1} KH_2PO_4, and *fourth row* 1.0 g l^{-1} KH_2PO_4. For each row, *first* and *second columns* correspond to the growth phase and production phase, respectively. *Dotted arrows* indicate flux toward biomass formation. Refer to legend of Fig. 1 for additional media components

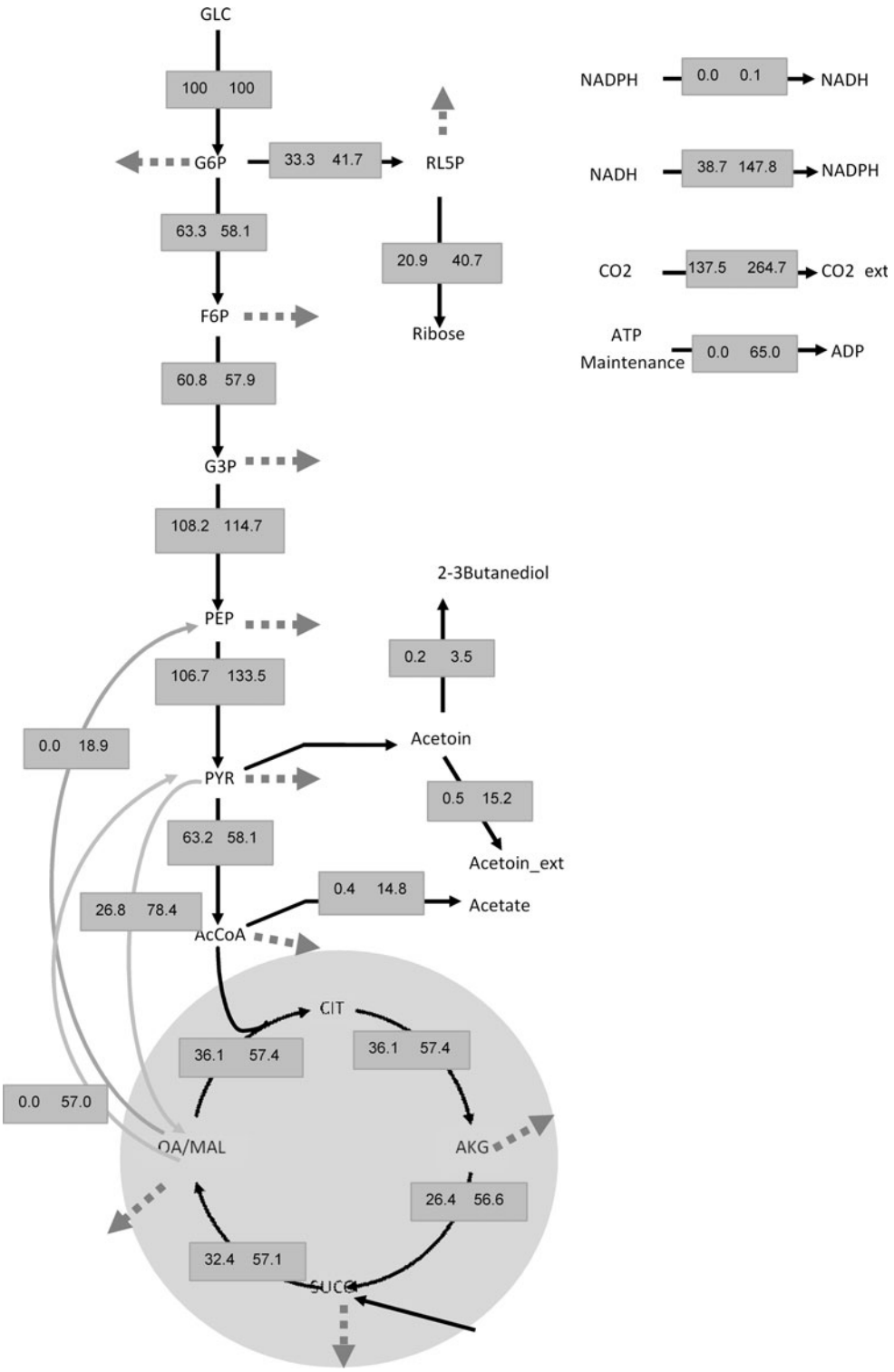

Fig. 6 Flux distribution of *B. pumilus* network in complex media containing 200 g l^{-1} glucose and 15 g l^{-1} casamino acid in shake flasks. For each row, *first* and *second columns* correspond to the growth phase and production phase, respectively. Additional medium components (in 1 l of distilled water): ammonium sulfate, 5 g; manganese sulfate, 0.5 g; calcium carbonate, 16.0 g

activities of malic enzyme and PEP carboxykinase are negligible in the growth phase and similar to values in the corresponding defined media. The flux through gluconeogenesis was absent in the first growth phase but showed an increase in the second phase.

Discussion

In this article, we have presented a simple methodology for the estimation of intracellular reaction rates in a transketolase deficient mutant strain of *B. pumilus* ATCC 21951.

The method requires only the substrate uptake, metabolite secretion rate, and biomass growth rate to be measured for accurate determination of flux partitioning at some of the key branch points in the central carbon metabolic network. Flux analysis was performed for the strain under a variety of growth conditions in both the growth phase and production phase. The intracellular flux distribution was significantly influenced by the concentrations of glucose, inorganic phosphate, amino acids, and dissolved oxygen in the media. This also resulted in alterations in D-ribose productivity. The bow-tie architecture of the central carbon metabolism has the potential to provide flexibility to the metabolic network and it was described in detail by Csete and Doyle in 2004 [9]. Identification and analysis of the bow-tie architecture in a metabolic network is a necessary prerequisite to understand the complex biologic processes. To this end flexibility of the metabolic network was evaluated at some of the important branch points. Both the absolute and relative values of the fluxes were affected by the medium composition. For example, the catabolic flux partitioning between glycolysis and the PPP at the G6P branch point was highly flexible. In a flexible node, enzymes participating in each branch show similar affinity for the node metabolite. The flux through each branch is controlled by feedback inhibition by the corresponding terminal metabolite [52]. The glucose-6-phosphate dehydrogenase, the first enzyme of the PP pathway is inhibited by the end product, NADPH. Phosphofructokinase, an enzyme of the glycolysis pathway, is also inhibited by high levels of ATP, which is produced in the glycolysis pathway. However, as a result of the transketolase deficiency, the PP pathway in the mutant *B. pumilus* strain is incomplete and therefore does not contribute to the production of the biomass precursors such as aromatic amino acids through the PP pathway. So there is no tight regulation of growth by the PP pathway in this strain. Another important observation is that the NADPH is produced not only by the PP pathway, but also through the NADPH-dependent malic enzyme. Note that in general, NADPH is found to be present in excess for *B. subtilis*, a strain that is related to *B. pumilus* [10, 39, 61]. This suggests that the flux through the PP pathway is not determined by the requirements for the redox cofactor NADPH in *B. pumilus*. Thus, the G6P node is flexible and the split ratio at this node has the potential to be modified. Possibly, this gives the cell the flexibility to regulate the energy and intermediate fluxes under environmental perturbations. This observation is contrary to that made by Fischer and Sauer [19] for *B. subtilis*: these authors found flux partitioning around the G6P node to be robust to genotypic alterations in the metabolic network. We observed some additional flexibility in the network of *B. pumilus* ATCC 21951 when we analyzed the anabolic biomass production and catabolic product/by-product formation around a pseudo-branch point. One may argue that the flexibility around the G6P branch point may have been the underlying reason for this *B. pumilus* strain to be selected from thousands of other strains in a screening for D-ribose producers conducted in the 1970s.

The flux partitioning between citrate synthase and acetate kinase around the AcCoA branch point was found to be robust against the changing environmental conditions. Likewise, the PYR branch point was found to be rigid to the environmental conditions. This rigid control architecture seems to be a built-in feature of the enzyme kinetics at some of the branch points. As a result, the formation of some of the by-products such as acetate and acetoin was unavoidable under conditions that favored D-ribose production. The maintenance flux, estimated in terms of mmole of ATP consumed per gram of biomass per hour, was found to be higher in the production phase compared to the growth phase. This is in agreement with previous reports of a higher ATP requirement for slow-growing cultures [32, 54]. Further, we observe that there is significantly excess formation of NADH and as a result, the transhydrogenase activity is high in the reverse direction from NADH to NADPH in all cases. It has been shown that at 5 % DO with a glucose concentration of 40, 100, and 200 g l^{-1} (glucose/DO ratio is 8, 20, and 40, respectively), *tkt* deficient *B. pumilus* produced ribose and pentose phosphate was active. But at 40 % DO with 100 g l^{-1} glucose (glucose/DO ratio was 2.5), ribose was not produced; whereas with 200 g l^{-1} glucose (glucose/DO ratio was 5), ribose was produced and pentose phosphate was active. If the glucose/DO ratio is high ribose is produced. This feature indicates that the flux to the PPP in *tkt* deficient *B. pumilus* not only depends on glucose concentration or DO but it also depends on glucose/DO ratio. This indicates that at higher DO, higher glucose is required in media to keep the PPP active and maintain ribose production. Higher DO represses the glucose-6-phosphate dehydrogenase and 6-phosphogluconate, the first and next enzymes of the PP pathway, respectively [56]. This effect may be due to the presence of oxygen free radicals which are normally generated in aerobic fermentation [15]. But microorganisms can produce antioxidants to reduce the free radicals. Even transketolase itself can protect against free radical oxidative stress [17] and keeps the PPP active. But in *tkt* deficient *B. pumilus* its antioxidant facility is hampered due to the lack of transketolase and therefore it is more prone to decrease the PP pathway activity at higher DO. Although glucose is a very weak antioxidant, at higher concentration it can nevertheless act as an effective antioxidant [21]. Therefore at 200 g l^{-1} glucose and 40 % DO, glucose acts as an antioxidant and therefore the PPP was active, whereas 100 g l^{-1} glucose may be insufficient at 40 % DO to act as an effective antioxidant. Therefore the

low value of glucose/DO ratio implies that the PPP is not highly active in transketolase deficient *B. pumilus*. Different phenomena have been observed in some other organisms where PPP flux depends on dissolved oxygen and glucose separately [20]. The method described in the present study is suitable for flux analysis for both growth and production phases assuming pseudo-steady-state conditions. This assumption is valid for exponential growth phase, but may not be so for production phase. Further, this method can be extended to non-steady-state conditions by using a dynamic profile of exchange rate becasuse an intracellular pseudo-steady state can be assumed during the transient culture as described by Lequeux et al. [24]. It should be noted that there are some limitations to flux analysis without using ^{13}C isotopic measurement, e.g., problems with parallel metabolic, cyclic, bidirectional, and split pathways. Some of these issues are addressed by incorporating cofactor balance in the flux balance model. Using the proposed method, we estimated the fluxes with high confidence. Further, this confidence limit is explicitly computed by using percentile methods.

Acknowledgments The work was partially supported by a grant from the Department of Biotechnology, Ministry of Science and Technology, Government of India.

References

1. Bapat PM, Das D, Sohoni SV, Wangikar PP (2006) Hierarchical amino acid utilization and its influence on fermentation dynamics: rifamycin B fermentation using *Amycolatopsis mediterranei* S699, a case study. Microb Cell Fact 5:32
2. Bapat PM, Wangikar PP (2004) Optimization of rifamycin B fermentation in shake flasks via a machine-learning-based approach. Biotechnol Bioeng 86(2):201–208
3. Barat M, Anagnostopoulos C, Schneider AM (1965) Linkage relationships of genes controlling isoleucine, valine and leucine biosynthesis in *Bacillus subtilis*. J Bacteriol 90:357–369
4. Baumberg S, Klingel U (1993) Biosynthesis of arginine, proline, and related compounds. In: Sonenshein AL, Hoch JA, Lorich R (eds) *Bacillus subtilis* and other grampositive bacteria: biochemistry, physiology, and molecular genetics. American Society for Microbiology, Washington, pp 299–306
5. Borodina I, Krabben P, Nielsen J (2005) Genome-scale analysis of Streptomyces coelicolor A3(2) metabolism. Genome Res 15(6):820–829
6. Calik P, Ozdamar TH (1999) Mass flux balance-based model and metabolic pathway engineering analysis for serine alkaline protease synthesis by *Bacillus licheniformis*. Enzyme Microbial Technol 24(10):621–635
7. Christensen B, Gombert AK, Nielsen J (2002) Analysis of flux estimates based on C-13-labelling experiments. Eur J Biochem 269(11):2795–2800
8. Cooper RA (1984) Metabolism of methylglyoxal in microorganisms. Ann Rev Microbiol 38:49–68
9. Csete M, Doyle J (2004) Bow ties, metabolism and disease. Trends Biotechnol 22(9):446–450
10. Dauner M, Storni T, Sauer U (2001) *Bacillus subtilis* metabolism and energetics in carbon-limited and excess-carbon chemostat culture. J Bacteriol 183(24):7308–7317
11. DeWulf P, Soetaert W, Schwengers D, Vandamme EJ (1996) Screening and mutational improvement of a D-ribose secreting Candida pelliculosa strain. J Ferment Bioeng 82(1):1–7
12. DeWulf P, Vandamme EJ (1997) Production of D-ribose by fermentation. Appl Microbiol Biotechnol 48(2):141–148
13. Dogan G (2007) Bootstrapping for confidence interval estimation and hypothesis testing for parameters of system dynamics models. Syst Dynam Rev 23(4):415–436
14. Duarte NC, Palsson BO, Fu PC (2004) Integrated analysis of metabolic phenotypes in Saccharomyces cerevisiae. BMC Genomics 5
15. Dumitru IF, Nechifor MT (1994) Decrease in yeast glucose-6-phosphate-dehydrogenase activity due to oxygen-free radicals. Int J Biochem 26(2):229–233
16. Edwards JS, Ramakrishna R, Schilling CH, Palsson BO (1999) Metabolic flux balance analysis. In: Lee SY, Papoutsakis ET (eds) Metabolic engineering. Marcel Deker, New York, pp 13–57
17. Estey T, Lassen N, Pappa A, Vasiliou V (2005) ALDH3A1 Is a multifunctional protein that protect against oxidative damage. In: Weiner H, Plapp B, Lindahl R, Maser E (eds) Enzymology and molecular biologyof carbonylmetabolism, vol 12. Purdue University Press, West Lafayette, pp 50–55
18. Ferguson GP, Totemeyer S, MacLean MJ, Booth IR (1998) Methylglyoxal production in bacteria: suicide or survival? Archiv Microbiol 170(4):209–219
19. Fischer E, Sauer U (2005) Large-scale in vivo flux analysis shows rigidity and suboptimal performance of *Bacillus subtilis* metabolism. Nat Gen 37(6):636–640
20. Fredlund E, Blank LM, Schnurer J, Sauer U, Passoth V (2004) Oxygen- and glucose-dependent regulation of central carbon metabolism in Pichia anomala. Appl Environ Microbiol 70(10):5905–5911
21. Giangiacomo A, Olesen PR, Ortwerth BJ (1996) Ascorbic acid and glucose oxidation by ultraviolet A-generated oxygen free radicals. Investigat Ophthalmol Visual Sci 37(8):1549–1556
22. Jackson JB, Cotton NPJ, Williams R, Bizouarn T, Hutton MN, Sazanov LA, Thomas CM (1993) Proton-translocating transhydrogenase in bacteria. Biochem Soc Trans 21(4):1010–1013
23. Kintaka K, Sekitani YH, Yamguchi JP (1986) Verfahrung zur Erzeugung von D-Ribose. German Patent DE 3524549A1 Patent German Patent. DE 3524549A1
24. Lequeux G, Beauprez J, Maertens J, Van Horen E, Soetaert W, Vandamme E, Vanrolleghem PA (2010) Dynamic metabolic flux analysis demonstrated on cultures where the limiting substrate is changed from carbon to nitrogen and vice versa. J Biomed Biotechnol 2010:19
25. Leven PA, Clarck EP (1921) D-Ribohexaminic. J Biol Chem 46:19–33
26. Maiti SK, Lantz AE, Bhushan M, Wangikar PP (2011) Multi-objective optimization of glycopeptide antibiotic production in batch and fed batch processes. Bioresour Technol 102(13): 6951–6958
27. Moore S (1968) Amino acid analysis: aqueous dimethyl sulfoxide as solvent for the ninhydrin reaction. J Biol Chem
28. Nielsen J (1998) Metabolic engineering: techniques for analysis of targets for genetic manipulations. Biotechnol Bioeng 58(2–3): 125–132
29. Park YC, Kim SG, Park K, Lee KH, Seo JH (2004) Fed-batch production of D-ribose from sugar mixtures by transketolase-deficient *Bacillus subtilis* SPK1. Appl Microbiol Biotechnol 66(3):297–302
30. Pasternak CA (1962) Sulphate activation and its control in *Escherichia coli* and *Bacillus subtilis*. Biochem J 85:44–49

31. Paulus H (1993) Biosynthesis of aspartate family of amino acids. In: Sonenshein AL, Hoch JA, Lorich R (eds) *Bacillus subtilis* and other gram-positive bacteria: biochemistry, physiology, and molecular genetics. American Society for Microbiology, Washington, pp 237–267
32. Pirt SJ (1982) Maintenance energy—a general-model for energy-limited and energy-sufficient growth. Arch Microbiol 133(4): 300–302
33. Reed JL, Vo TD, Schilling CH, Palsson BO (2003) An expanded genome-scale model of *Escherichia coli* K-12 (iJR904 GSM/GPR). Genome Biol 4(9):R54
34. Sasajima K, Kumada T (1981) Cell surface change of *Bacillus subtilis* pleiotropic mutant lacking transketolase. Inst Ferment Res Commun 10:3–9
35. Sasajima K, Yokota A, Kumada T (1985) Alteration of the membrane compostion of *Bacillus subtilis* pleiotropic mutant lacking transketolase. Inst Ferment Res Commun 12:5–18
36. Sasajima K, Yoneda M (1989) Production of D-ribose by microorganisms. In: Vandamme EJ (ed) Biotechnology of vitamins, pigments and growth factors. Elsevier, New York, pp 167–197
37. Sauer U, Bailey JE (1999) Estimation of P-to-O ratio in *Bacillus subtilis* and its influence on maximum riboflavin yield. Biotechnol and Bioeng 64(6):750–754
38. Sauer U, Cameron DC, Bailey JE (1998) Metabolic capacity of *Bacillus subtilis* for the production of purine nucleosides, riboflavin, and folic acid. Biotechnol Bioeng 59(2):227–238
39. Sauer U, Hatzimanikatis V, Bailey JE, Hochuli M, Szyperski T, Wuthrich K (1997) Metabolic fluxes in riboflavin-producing *Bacillus subtilis*. Nat Biotechnol 15(5):448–452
40. Sauer U, Lasko DR, Fiaux J, Hochuli M, Glaser R, Szyperski T, Wuthrich K, Bailey JE (1999) Metabolic flux ratio analysis of genetic and environmental modulations of *Escherichia coli* central carbon metabolism. J Bacteriol 181(21):6679–6688
41. Schilling CH, Covert MW, Famili I, Church GM, Edwards JS, Palsson BO (2002) Genome-scale metabolic model of *Helicobacter pylori* 26695. J Bacteriol 184(16):4582–4593
42. Schuetz R, Kuepfer L, Sauer U (2007) Systematic evaluation of objective functions for predicting intracellular fluxes in *Escherichia coli*. Mol Syst Biol 3:119
43. Skolpap W, Nuchprayoon S, Scharer JM, Moo-Young M (2007) Parametric analysis of metabolic fluxes of alpha-amylase and protease-producing *Bacillus subtilis*. Bioproc Biosyst Eng 30(5):337–348
44. Smith DCC (1955) The preparation of D-ribose and 2-deoxy-D-ribose from glucose. Chem Ind 1955:92–93
45. Sonenshein AL (1993) Introduction to metabolic pathways. In: Sonenshein AL, Hoch JA, Lorich R (eds) *Bacillus subtilis* and other gram-positive bacteria: biochemistry, physiology, and molecular genetics. American Society for Microbiology, Washington, pp 127–132
46. Srivastava RK, Jaiswal R, Panda D, Wangikar PP (2008) Megacell Phenotype and its relation to metabolic alterations in transketolase deficient strain of *Bacillus pumilus*. Biotechnol Bioeng 102(5):1387–1397
47. Srivastava RK, Wangikar PP (2008) Combined effects of carbon, nitrogen and phosphorus substrates on D-ribose production via transketolase deficient strain of *Bacillus pumilus*. J Chem Technol Biotechnol 83(8):1110–1119
48. Stephanopoulos G (2002) Metabolic engineering: perspective of a chemical engineer. AIChE J 48(5):920–926
49. Stephanopoulos G, Alper H, Moxley J (2004) Exploiting biological complexity for strain improvement through systems biology. Nat Biotechnol 22(10):1261–1267
50. Stephanopoulos G, Aristidou AA, Nielsen J (1998) Metabolic engineering-principles and methodologie. Academic, San Diago
51. Stephanopoulos G, Simpson TW (1997) Flux amplification in complex metabolic networks. Chem Eng Sci 52(15):2607–2627
52. Stephanopoulos G, Vallino JJ (1991) Network rigidity and metabolic engineering in metabolite overproduction. Science 252(5013):1675–1681
53. Suzuki T, Tanaka N, Tomita F, Mizuhara K, Kinoshita S (1963) Bacterial accumulation of ribose and ribose-5-phosphate. J Appl Gen Microbiol 9:457–458
54. Takac S, Calik G, Mavituna F, Dervakos G (1998) Metabolic flux distribution for the optimized production of L-glutamate. Enzyme Microbial Technol 23(5):286–300
55. Tannler S, Decasper S, Sauer U (2008) Maintenance metabolism and carbon fluxes in *Bacillus* species. Microbial Cell Factories 7
56. Thomas AD, Doelle HW, Westwood AW, Gordon GL (1972) Effect of oxygen on several enzymes involved in the aerobic and anaerobic utilization of glucose in *Escherichia coli*. J Bacteriol 112(3):1099–1105
57. Vallino JJ, Stephanopoulos G (1994) Carbon flux distributions at the glucose-6-phosphate branch point in corynebacterium-glutamicum during lysine overproduction. Biotechnol Prog 10(3): 327–334
58. Varma A, Palsson BO (1994) Metabolic flux balancing—basic concepts, scientific and practical use. Nat Biotechnol 12(10): 994–998
59. Weber J, Kayser A, Rinas U (2005) Metabolic flux analysis of *Escherichia coli* in glucose-limited continuous culture. II. Dynamic response to famine and feast, activation of the methylglyoxal pathway and oscillatory behaviour. Microbiology 151:707–716
60. Wiechert W (2001) C-13 metabolic flux analysis. Metabol Eng 3(3):195–206
61. Zamboni N, Fischer E, Muffler A, Wyss M, Hohmann HP, Sauer U (2005) Transient expression and flux changes during a shift from high to low riboflavin production in continuous cultures of *Bacillus subtilis*. Biotechnol Bioeng 89(2):219–232
62. Zimmer HG (1992) The oxidative pentose-phosphate pathway in the heart—regulation, physiological significance, and clinical implications. Basic Res Cardiol 87(4):303–316